ISSN 1392-1320 MATERIALS SCIENCE (MEDŽIAGOTYRA). Vol. 30, No. 2. 2024

Fabrication of High-Performance Insulated Metal Substrates Employing h-BN Mixture/Epoxy Composite Coated on Roughened Copper Plate

Zhigang LI [1], Yigang HE [1], Hao ZHAO [2], Jianyu WU [2], Zhenbo ZHAO [2] *

[1] *School of Electrical Engineering and Automation, Hefei University of Technology, Hefei 230009, China*
[2] *Science and Technology on Reliability Physics and Application of Electronic Component Laboratory, China Electronic Product Reliability and Environmental Testing Research Institute, Guangzhou 511370, China*

http://doi.org/10.5755/j02.ms.34711

Received 25 July 2023; accepted 18 October 2023

In this work, an Insulated Metal Substrate (IMS) for packaging high-power electronic devices was created using hexagonal Boron Nitride (h-BN) mixture-based Thermally Conductive Adhesive (TCA) and copper plate with a matte side. Mechanical exfoliation of micron-scale BN particles results in a BN mixture containing h-BN nanosheets, micron particles, and nanoparticles. TCA was synthesized by dispersing a 40 % BN mixture modified by γ-aminopropyltriethoxysilane (KH550) into epoxy resin. The TCA has a relatively high thermal conductivity of 4.48 $W \cdot m^{-1} \cdot K^{-1}$ and a breakdown strength of 15.32 $kV \cdot mm^{-1}$. As the TCA film was coated on the matte side of the copper plate, the peel strength can reach 1.63 $N \cdot mm^{-1}$, indicating excellent practicality in the field of electronic packaging.

Keywords: insulated metal substrate, hexagonal boron nitride, epoxy resin, thermal conductivity, peel strength.

1. INTRODUCTION

As an Ultra-large-scale Integration (ULSI) circuit, a system on a chip (SoC) is a system-level chip with high integration, tiny size, and lightweight that meets the needs of miniaturization and lightweight [1 – 3]. It is now the most often used electronic component in equipment. The heat generated during device operation must be dissipated promptly in SoC-type devices to avoid decreasing device performance [4 – 6]. As a result, power modules require high-quality packaging substrates with good thermal conductivity and thermal dissipation [7 – 9].

A dielectric insulating layer and a thick metal substrate make up insulated metal substrates (IMSs). Thermally conductive ceramic particles and resin composites directly adhere to the copper substrate as insulation layers, and the chips are flipped on the insulation layer via the metalized circuit schematic [10]. Due to the IMSs employed in the packaging of high-power electronic devices, they must have not only great thermal conductivity but also outstanding insulation and mechanical strength. As a result, IMSs made of thermally conductive adhesives (TCAs) with highly thermally conductive insulating fillers and resins bonded to thick copper plates have substantial advantages.

TCAs often use ceramic fillers such as Al_2O_3, AlN, Si_3N_4, SiC, and BN particles [11 – 15]. Hexagonal BN (h-BN) has a graphene-like structure, resulting in an ultrahigh theoretical thermal conductivity in in-plane BN of up to 2000 $W \cdot m^{-1} \cdot K^{-1}$ [16]. TCAs with BN nanosheets exfoliated from h-BN particles as filler have the best thermal conductivity in theory. However, the smooth surface of the BN nanosheets makes it difficult to evenly disperse in the resin, lowering the overall performance of TCAs containing only BN nanosheets [17].

Aluminum and copper plates are ideal metal substrates for TCAs because they are highly thermally conductive, and copper has a higher chemical stability and corrosion resistance than aluminum. Hence, copper is the most often used metal substrate for TCAs [18]. The binding strength of the TCA to the copper substrate is a critical parameter that is directly related to the mechanical qualities and thermal performance of IMSs. Because the interaction between the resin compound and the copper substrate is mostly physical, the bonding area is greatly increased in favor of the bonding strength [19].

In this work, commercial h-BN particles were exfoliated to prepare a BN mixture of micron-scale BN particles, nanoscale BN particles, and BN nanosheets. As the BN mixture was employed as the filler to synthesize the TCSs, the BN particles could be filled up to 40 % in the TCAs, effectively improving the thermal conductivity of the TCAs. Furthermore, this work employed electrodeposition to grow copper islands on the surface of the copper plate, which greatly improved the peel strength of the TCAs on the copper plate. The prepared IMSs are extremely useful in the packing of high-power electronic equipment.

2. EXPERIMENTAL

2.1. Materials preparation

In a typical procedure, an electrolytic copper plate (Runde Metal, China) with a purity of 99.99 % and a size of 1 mm × 100 mm × 100 mm experienced pre-treatment, including electrochemical degreasing and corrosion process. Firstly, the copper plate was electrochemically degreased in a cathode with a current density of 10 $A \cdot dm^{-2}$ at 70 °C for 1 min. The corrosion solution contains 100 $g \cdot l^{-1}$ of H_2SO_4 and 100 $g \cdot l^{-1}$ of $Fe_2(SO_4)_3$ and the corrosion was carried out

* Corresponding author. Tel.: +086-18898432101.
E-mail: *zhaozb@ceprei.com* (Z. Zhao)

at room temperature for 1 min. Afterward, the copper plate was plated with copper islands, and the copper islands were plated with copper. The rough copper layer (matte side) with copper islands was electrodeposited for 1 minute at 50 °C in an electrolyte solution containing 80 $g·l^{-1}$ of $CuSO_4·5H_2O$, 5 $g·l^{-1}$ of $CuCl_2$, and 100 $g·l^{-1}$ of H_2SO_4, with the current density approximatively controlled at 25 $A·dm^{-2}$. Considering the low binding force between the produced copper islands and copper substrate, the sample was promptly electrodeposited with copper at a relatively low current density of 10 $A·dm^{-2}$ in a plating bath copper containing 250 $g·l^{-1}$ of $CuSO_4·5H_2O$ and 50 $g·l^{-1}$ of H_2SO_4 at 50 °C for 20 s. The above-mentioned chemicals were purchased from Tianjin Kemiou Chemical Reagent Co., China.

To prepare a BN mixture, commercial h-BN particles were exfoliated using a high shear disperse homogenizing emulsification machine (B25 model, BRT Technology, Shanghai China) at 70 °C. First, 2.5 g of b-BN particles were dispersed in an appropriate volume of N-methylpyrrolidone, and the dispersion was heated in an oil bath at 60 °C overnight under intensive stirring. Then, the dispersion was exfoliated with a High Shear Disperse Homogenizing Emulsification Machine for different times (5, 10, and 15 h) in a water bath at 70 °C under stirring. Thereafter, the resulting dispersion was centrifuged at 8000 rpm, repeatedly washed with ethanol 3 times, and dried in a vacuum at 80 °C.

The exfoliated BN mixture was mixed with a 5:2 mass ratio of epoxy adhesive comprised of triethanolamine and bisphenol F epoxy resin (NPEF-170). After uniformly stirring, the TCA was placed in defoaming tanks and de-foamed in a de-foamer (SIE-CV300, Guangzhou SIENOX, China) at 1500 revolutions per minute (rpm) for 10 min at room temperature. The TCA was then coated on the matte side of the copper plate using a spin coating method in a spinner at 5000 rpm for 30 s. Finally, the coated TCA was cured and heat-treated in a muffle furnace at 250 °C for 2 h.

2.2. Characterisations and performance tests

X-ray diffraction (XRD, a Philips Xpert, Philips, Netherlands) was used to analyze the crystal structure of the copper plate and BN materials. Scanning electron microscopy (SEM) was employed on the samples to investigate their morphology using a Phenom Pro scanning electron microscope (Phenom Scientific, Shanghai, China). The surface roughness was investigated using a Surface Roughness Meter (TR200, Beijing Zhongyi Technology, China). A Benchtop Thermal Conductivity Meter (DRL-III, Shanghai Qunhong Instrument, China) was used to measure thermal conductivity. The breakdown voltage tester (HT-100, Shanghai Xuji Electric, China) performs the breakdown strength test. Peel strength testing was carried out using a Universal Tensile Testing Machine (XF-5KN, Xiamen XiongFa Instruments, China).

3. RESULTS AND DISCUSSION

Fig. 1 depicts the XRD patterns of commercial copper plate and our sample. The standard electrolytic copper peaks are visible on both the commercial copper plate and the roughened copper plate, which exhibits the preferred orientation of the (220) crystal surface [20]. It is also observed that the peak intensities of the commercial copper plate are higher than those of the roughened copper plate, suggesting that the rapid roughening results in the copper islands with lower crystallinity than the commercial copper plate.

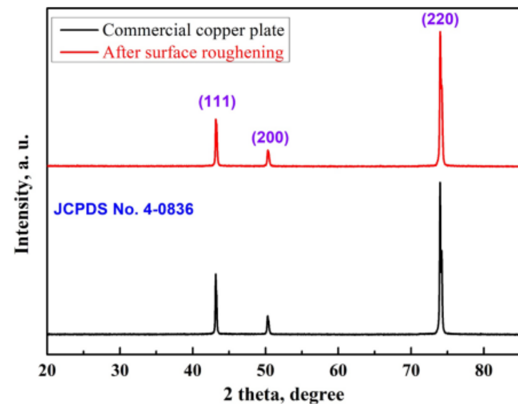

Fig. 1. XRD patterns of commercial and roughened copper plates

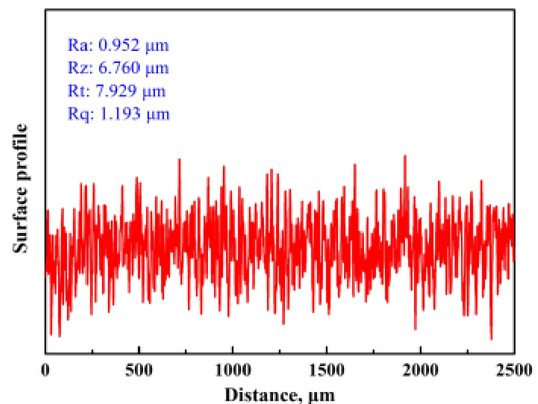

a

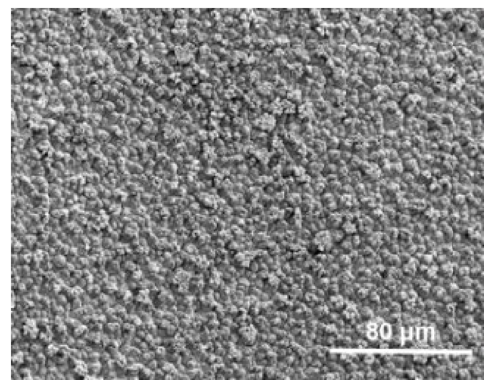

b

Fig. 2. a – surface profile of matte side; b – SEM image of the matte side of the prepared copper plate

Fig. 2 a shows the roughness test result of the prepared sample. The undulating curve demonstrates the formation of a matte side on a copper plate. The measured values for differently defined roughnesses including arithmetic average roughness (*R*a), maximum peak to valley height (*R*t), mean roughness depth (*R*z), and root mean square average (*R*q) are confirmed to be 0.952, 6.760, 7.929, and 1.193 μm, respectively. The rough surface aids in the adhesion of the TCA to the substrate, hence increasing the peel strength of the TCA on the copper plate [21].

Fig. 2 b shows an SEM image of the matte side of the prepared sample at low magnification, and the rough surface was confirmed. On the matte side of the copper plate, many small copper islands are uniformly scattered. Fig. 3 a is a high-magnification SEM image. The copper islands are clearly made up of microscopic copper particles ranging in size from 0.8 to 2 μm. Fig. 3 b shows a typical cross-section. The graphic shows a significant island-like structure, with copper islands ranging in height from 3 to 7 μm.

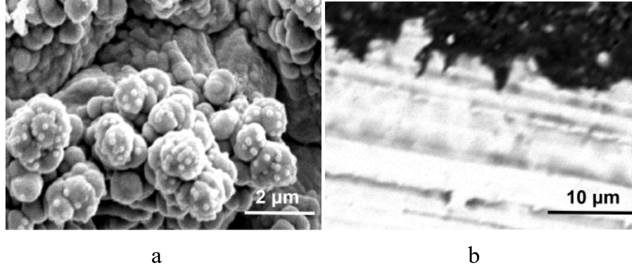

Fig. 3. a – SEM image of the matte side; b – SEM cross-section image of the roughed copper plate

Fig. 4 a shows an SEM image of commercial h-BN particles with a nominal size of 2 μm. The particles are observed a relatively uniform size of 1 ~ 1.5 μm. The SEM images of the exfoliated boron nitride particles at various times are shown in Fig. 4 b – d. When the exfoliating time is controlled for 5 h, the size of the BN particles is substantially lower than that of the commercial sample. The particle size distribution range widens and some aggregated particles appear in the samples. The large number of aggregates from the sample exfoliated for 10 h is readily visible in Fig. 4 c. Aggregates are made up of particles with varying particle sizes. Of course, the processed sample contains a significant number of small particles ranging in size from 100 to 500 nm, demonstrating the effectiveness of the exfoliating process. As the exfoliation time increases to 15 h, the boron nitride particles produce nearly tiny particles (Fig. 4 d). Despite ultrasonic dispersion, almost all of the tiny particles aggregate. The sample has a large specific surface area and a high surface Gibbs free energy due to the lack of surface modification by coupling agents and the newly generated BN tiny particles, as well as the lamellar structure, resulting in particle agglomeration to reduce the Gibbs free energy of the sample. As a result, BN particle aggregation is reasonable. Fig. 4 e depicts a typical TEM image of exfoliated BN particles. In the TEM image, numerous types of BN can be seen, including BN nanosheets, low-layer BN, multi-layer BN, and BN micro-meter scale and nano-scale particles of varied sizes, confirming that the synthetic material is a BN mixture. The laminar structure of BN appears to be formed from BN particles exfoliated by the High Shear Disperse Homogenizing Emulsification Machine, which also results in a reduction in BN particle size, which matches SEM data.

XRD patterns of commercial and exfoliated h-BN particles are shown in Fig. 5. Five notable peaks at 26.8°, 41.6°, 43.9°, 50.2°, and 55.2° can be attributed to the (002), (100), (101), (102), and (004) lattice planes [22]. It is important to note that, in contrast to the other peaks, the intensity of the (004) peak is barely reduced, implying that the exfoliating process causes almost no damage to the (004) crystal surface, which is similar to the result of the ball milling process for the treatment of BN particles [23].

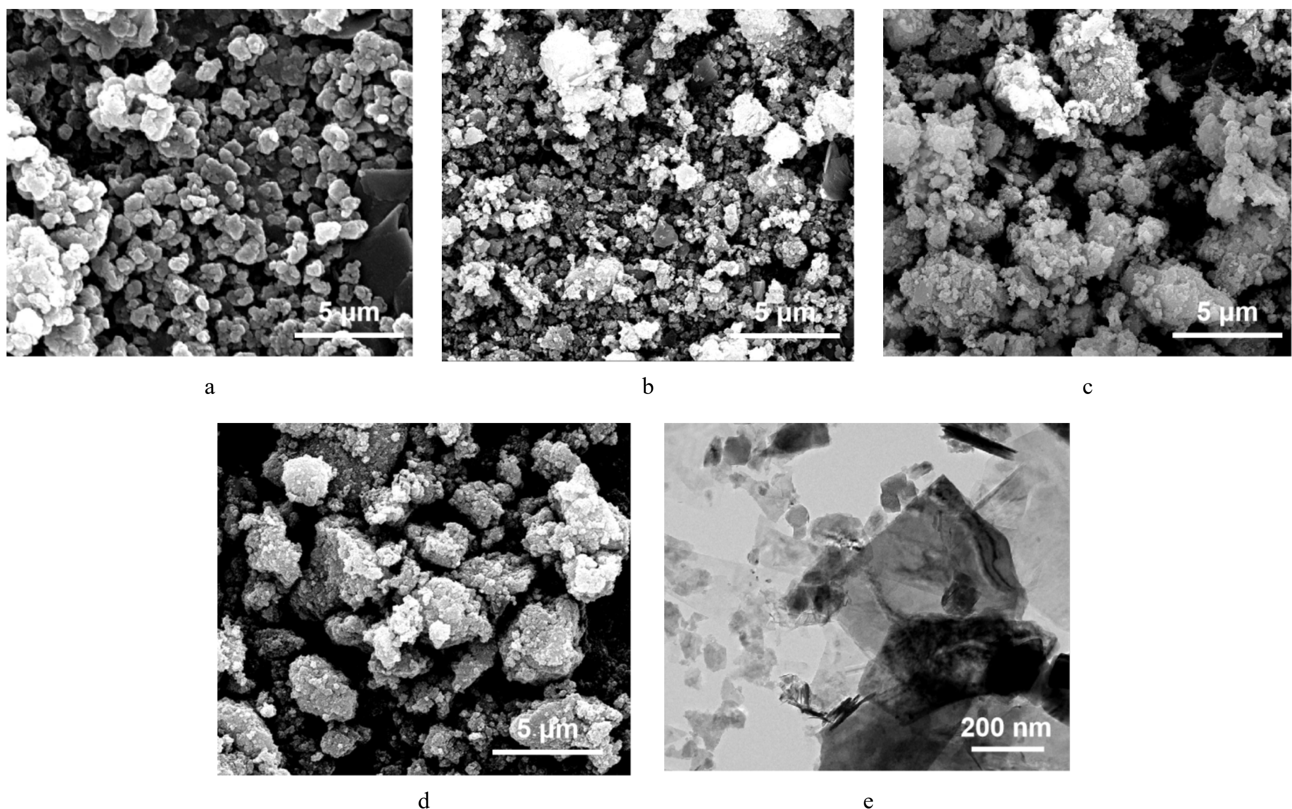

Fig. 4. a – SEM image of commercial h-BN particles; b – SEM image of h-BN particles exfoliated for 5 h; c – SEM image of h-BN particles exfoliated for 10 h; d – SEM image of h-BN particles exfoliated for 15 h; e – TEM image of BN particles exfoliated for 10 h

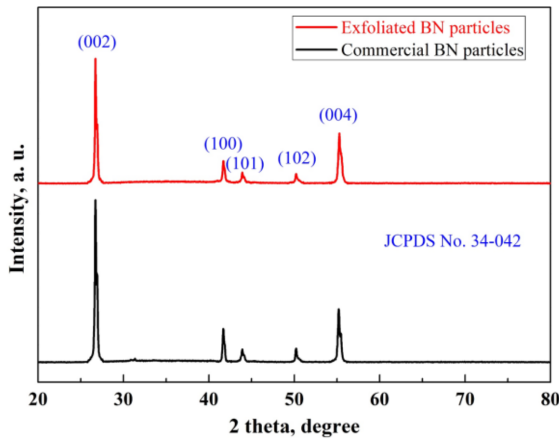

Fig. 5. XRD patterns of commercial h-BN particles and h-BN mixture

The other peaks simply reduce in intensity rather than vanish, showing the presence of BN particles with smaller grain sizes. The presence of multiple forms of h-BN in the sample is demonstrated by the SEM and XRD characterization of the exfoliated h-BN particles.

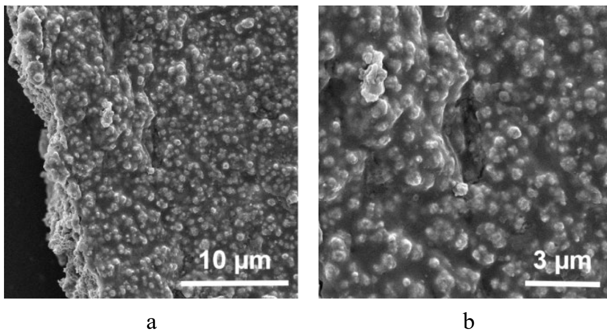

Fig. 6. SEM images of the TCA: a – low magnification; b – high magnification.

Fig. 6 shows SEM images of the TCA. The cured TCA with a high concentration (40 %) of BN particle filler has substantial particle undulations on its surface. BN particles treated with the KH550 coupling agent are dispersed more uniformly in the epoxy resin.

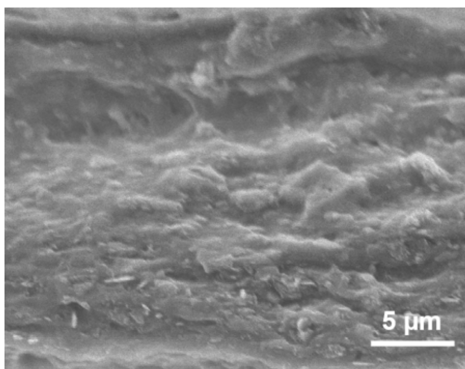

Fig. 7. SEM cross-section image of the TCA

Fig. 7 depicts a cross-section of the TCA, which further confirms the uniformity of particle distribution. Fig. 8 depicts the experimental results of a thermogravimetric examination of a TCA containing a 40 % h-BN mixture. According to the graph, the epoxy resin began to disintegrate around 400 °C and nearly completed the decomposition by 450 °C. The trend of the TG curve is consistent with previous references [17]. At 800 °C, the residual quantity is 41.3 %, with an additional 1.3 % coming from epoxy resin decomposition residue.

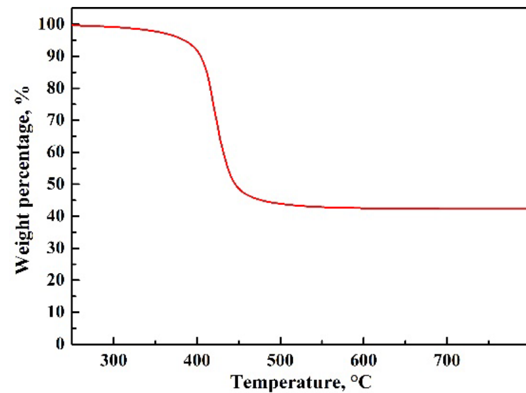

Fig. 8. Thermogravimetric curve of the prepared TCA

Thermal conductivities of TCAs with varying exfoliation durations and h-BN contents are illustrated in Fig. 9. Because of the strong thermal conductivity qualities of h-BN, all samples display a considerable rise in thermal conductivity with increasing h-BN content. Part of the micron-scale BN particles eventually changed into BN nanosheets and BN tiny particles as the exfoliation duration increased. It has been established that fillers made of a mixture of BN nanosheets and BN particles have a greater thermal conductivity of 4.48 $W \cdot m^{-1} \cdot K^{-1}$ than single nanosheet or BN particle fillers in a TCA. h-BN nanosheets and particles appear to make it easier to form a three-dimensional linked network structure in TCA, which improves thermal conductivity [24]. Although the BN mixture filler has been modified by the coupling agent when the exfoliating time is 15 h, the 40 % content makes it difficult to achieve uniform dispersion in the epoxy resin, and so the thermal conductivity is lower than that of the BN mixture filler when the exfoliating time is 10 h.

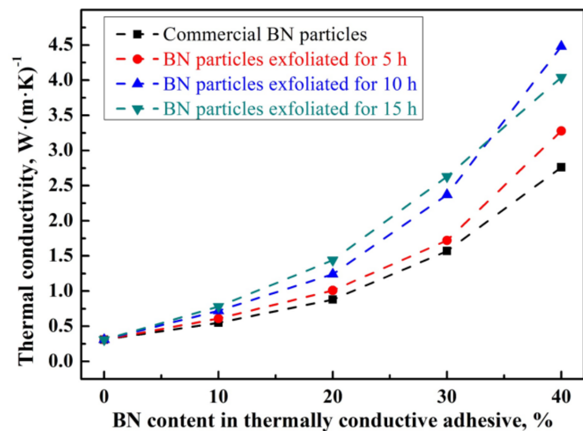

Fig. 9. Thermal conductivity dependence of h-BN content in TCA

Fig. 10 depicts the breakdown field strength of a TCA with varying h-BN filler concentrations. Mechanical methods were used to exfoliate h-BN particles into tiny particles and nanosheets, while a significant number of defects were produced on the surface of the tiny particles and at the edges of the nanosheets to stimulate the production of carriers. The generation of carriers improves

the thermal conductivity of the composite but not its breakdown strength. When the h-BN concentration is 10 %, the breakdown strength is maximal, and a downward trend appears. When the h-BN content is at a low level, it is expected to be uniformly disseminated in the epoxy resin, forming an excellent interfacial region that inhibits carrier migration. Furthermore, the breakdown strength of the epoxy matrix itself plays a significant impact in improving the breakdown strength. As the h-BN concentration increases, the distance between h-BN particles decreases, resulting in a shorter carrier migration distance and a drop in breakdown strength. When the percentage of the h-BN mixture reaches 40 %, the breakdown strength can still be kept at a high level of 15.32 kV·mm^{-1}.

The peel strength of TCAs on the copper substrate is critical. In this work, 35 μm copper foil was utilized instead of copper plates to evaluate the peel strength of the samples.

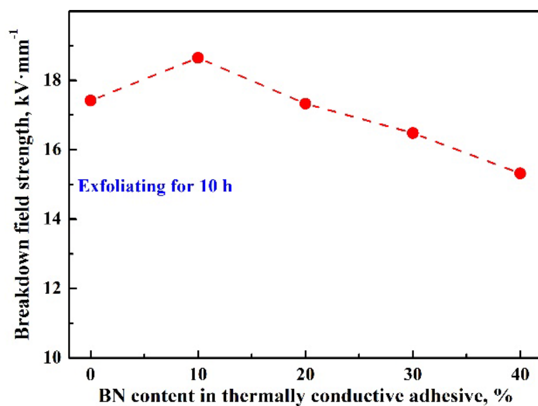

Fig. 10. Breakdown field strength dependence of h-BN content in TCA

Because of the high bending resistance of thick copper foil, peel strength testing is not practicable. The preparation procedure of copper islands on copper foil was the same as that of copper plates. The peel strength was determined on a Universal Tensile Testing Machine for the 90° stripping testing in accordance with the Chinese standard GB/T13557 (IPC-TM-650). Fig. 11 depicts a schematic showing the peel strength of a copper foil with copper islands developed on one side and a smooth copper foil on both sides.

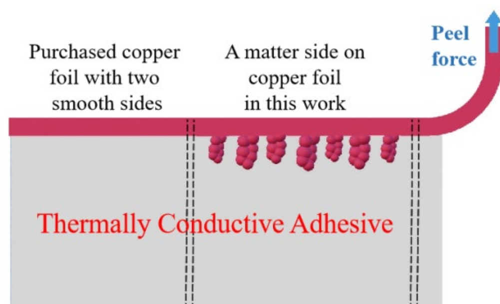

Fig. 11. Diagram of peel strength test experiments

During the test, the force direction is perpendicular to the tested copper foil and the bonding surface of the copper foil was pre-surface modified with KH550. In this investigation, the peel strength of the copper foil before rough treatment was 0.47 N·mm^{-1}, and after rough treatment to generate a matte side, the peel strength improved dramatically to 1.63 N·mm^{-1}. The rough surface allows for additional bonding area to the thermally conductive glue, while the granular copper islands resist vertical peeling force. The roughened copper foil appears to have great peel strength, which increases its practical value in packaging electronic components such as SoC-type devices.

4. CONCLUSIONS

A highly efficient IMS for high-power electronic device packing was successfully conceived and prepared. A BN mixture including nanosheets, micron-scale, and nano-scale particles was initially mechanically produced using a High Shear Disperse Homogenizing Emulsification Machine at 70 °C and 20000 rpm. The thermal conductivity of the IMS with varying BN content was measured. It is shown that increasing the BN content enhances the thermal conductivity of the TCA substantially. The TCA has improved heat conductivity and breakdown strength when the BN content is 40 %. By coating the TCA on the matte of a copper plate, a highly efficient IMS was successfully created, and the peel strength of up to 1.63 N·mm^{-1} is proven, demonstrating the viability of this IMS in electronic packaging for high-power devices.

Acknowledgments

This work was supported in part by the Key-Area Research and Development Program of Guangdong Province under Grant 2022B0701180002.

REFERENCES

1. **Xia, L., Cheng, J., Glover, N.E., Chiang, P.** 0.56 V, –20 dBm RF-powered, Multi-node Wireless Body Area Network System-on-a-chip with Harvesting-efficiency Tracking Loop *IEEE Journal of Solid-State Circuits* 49 (6) 2014: pp. 1345 – 1355. http://dx.doi.org/10.1109/JSSC.2014.2305074
2. **Anders, J., Dreyer, F., Krueger, D., Schwartz, I., Plenio, M.B., Jelezko, F.** Progress in Miniaturization and Low-Field Nuclear Magnetic Resonance *Journal of Magnetic Resonance* 322 2021: pp. 106860. https://doi.org/10.1016/j.jmr.2020.106860
3. **Ahmed, F.U., Sandhie, Z.T., Ali, L., Chowdhury, M.H.** A Brief Overview of On-Chip Voltage Regulation in High-Performance and High-Density Integrated Circuits *IEEE Access* 9 2021: pp. 813 – 826. https://doi.org/10.1109/ACCESS.2020.3047347
4. **Kim, S., Kim, J., Kim, J.H.** Fabrication of Insulated Metal Substrates with Organic Ceramic Composite Films for High Thermal Conductivity *Ceramics International* 43 |2017: pp. 8294 – 8299. http://dx.doi.org/10.1016/j.ceramint.2017.03.163
5. **Wang, L., Yang, C., Wang, X., Shen, J., Sun, W., Wang, J., Yang, G., Cheng, Y., Wang, Z.** Advances in Polymers and Composite Dielectrics for Thermal Transport and High-Temperature Applications *Composites Part A: Applied Science and Manufacturing* 164 2023: pp. 107320. https://doi.org/10.1016/j.compositesa.2022.107320
6. **Xiong, C., Wang, Y., Lin, L., Gao, M., Huang, Y., Chu, P.** Deposition of Nanocomposites Coating on Polyimide Films by Atmospheric Pressure Plasma for Enhanced Thermal Conductivity *Surfaces and Interfaces* 37 2023: pp. 102758. https://doi.org/10.1016/j.surfin.2023.102758

7. **Moore, A.L., Shi, L.** Emerging Challenges and Materials for Thermal Management of Electronics *Materials Today* 17 (4) 2014: pp. 163 – 174. https://doi.org/10.1016/j.mattod.2014.04.0031
8. **Du, J., Dai, W., Kou, H., Wu, P., Xing, W., Zhang, Y., Zhang, C.** AlN Coatings with High Thermal Conductivity and Excellent Electrical Properties for Thermal Management Devices *Ceramics International* 49 (11) 2023: pp. 16740 –16752. https://doi.org/10.1016/j.ceramint.2023.02.035
9. **Mena-Garcia, J., Ndayishimiye, A., Fan, Z., Perini, S.E., Li, W., Poudel, B., Priya, S., Foley, B., Gaskins, J., Randall, C.A.** Sodium Molybdate-Hexagonal Boron Nitride Composites Enabled by Cold Sintering for Microwave Dielectric Substrates Journal of the American Ceramic Society 2023: pp. 1 – 23. https://doi.org/10.1111/jace.19254
10. **Liu, E., Conti, F., Bhogaraju, S.K., Signorini, R., Pedron, D., Wunderle, B., Elger, G.** Thermomechanical Stress in GaN-LEDs Soldered onto Cu Substrates Studied Using Finite Element Method and Raman Spectroscopy *Journal of Raman Spectroscopy* 51 2020: pp. 2083 – 2094. https://doi.org/10.1002/jrs.5947
11. **Alim, M.A., Abdullah, M.Z., Aziz, M.S.A., Kamarudin, R., Gunnasegaran, P.** Recent Advances on Thermally Conductive Adhesive in Electronic Packaging: A Review *Polymers* 13 (19) 2021: pp. 1 – 23. https://doi.org/10.3390/polym13193337
12. **Tang, B., Wei, H., Zhao, D., Zhang, S.** Light-Heat Conversion and Thermal Conductivity Enhancement of PEG/SiO_2 Composite PCM by in Situ Ti_4O_7 Doping *Solar Energy Materials Solar Cells* 161 2017: pp. 183 – 189. https://doi.org/10.1016/j.solmat.2016.12.003
13. **Chen, C., Xue, Y., Li, X., Wen, Y., Liu, J., Xue, Z., Shi, D., Zhou, X., Xie, X., Mai, Y.** High-Performance Epoxy/Binary Spherical Alumina Composite as Underfill Material for Electronic Packaging *Composites Part A – Applied Science Manufacturing* 118 2019: pp. 67 – 74. https://doi.org/10.1016/j.compositesa.2018.12.019
14. **Cho, Y., Kim, J.** Effects of Two Silane Surface Modifications with Different Functional Groups on the Thermal Conductivity and Mechanical Properties of UV-Cured Composites with High Ceramic Filler Loading *Ceramics International* 48 (21) 2022: pp. 32001 – 32008. https://doi.org/10.1016/j.ceramint.2022.07.137
15. **Feng, Q.-K., Liu, C., Zhang, D.L., Song, Y.H., Sun, K., Xu, H.-P., Dang, Z.-M.** Particle Packing Theory Guided Multiscale Alumina Filled Epoxy Resin with Excellent Thermal and Dielectric Performances *Journal of Materiomics* 8 2022: pp. 1058 – 1066. https://doi.org/10.1016/j.jmat.2022.02.0
16. **Lin, Z., Mcnamara, A., Liu, Y., Moon, K.-S, Wong, C.-P.** Exfoliated Hexagonal Boron Nitride-based Polymer Nanocomposite with Enhanced Thermal Conductivity for Electronic Encapsulation *Composites Science and Technology* 90 2014: pp. 123 – 128. https://doi.org/10.1016/j.compscitech.2013.10.018
17. **Meng, Q., Han, S., Liu, T., Ma, J., Ji, S., Dai, J., Kang, H., Ma, J.** Noncovalent Modification of Boron Nitrite Nanosheets for Thermally Conductive, Mechanically Resilient Epoxy Nanocomposites *Industrial & Engineering Chemistry Research* 59 (47) 2020: pp. 20701 – 20710. https://dx.doi.org/10.1021/acs.iecr.0c03133
18. **Gurpinar, E., Chowdhury, S., Ozpineci, B., Fan, W.** Graphite-Embedded High-Performance Insulated Metal Substrate for Wide-Bandgap Power Modules *IEEE Transactions on Power Electronics* 36 2021: pp. 114 – 128. https://doi.org/10.1109/TPEL.2020.3001528
19. **Tsurumi, N., Tsuji, Y., Baba, T., Murata, H., Masago, N., Yoshizawa, K.** Comparative Study of the Ideal and Actual Adhesion Interfaces of the Die Bonding Structure Using Conductive Adhesives *The Journal of Adhesion* 98 (1) 2022: pp. 24 – 48. https://doi.org/10.1080/00218464.2020.1807958
20. **Wang, N., Chen, Q., Gong, X., Hu, W.** Electrochemical Double-pulse Technique to Modulate the Roughened Surface of Copper Foil for Copper-clad Laminates *Transactions of the Institute of Metal Finishing* 100 (5) 2022: pp. 276 – 282. https://doi.org/10.1080/00202967.2022.2059847
21. **Jia, L., Yang, H., Wang, Y., Zhang, B., Liu, H., Hao, J.** Direct Bonding of Copper Foil and Liquid Crystal Polymer by Laser Etching and Welding *Optics and Lasers in Engineering* 139 2021: pp. 106509. https://doi.org/10.1016/j.optlaseng.2020.106509
22. **Kim, K., Ju, H., Kim, J.** Filler Orientation of Boron Nitride Composite via External Electric Field for Thermal Conductivity Enhancement *Ceramics International* 42 (7) 2016: pp. 8657 – 8663. https://doi.org/10.1016/j.ceramint.2016.02.098
23. **Li, L.H., Chen, Y., Cheng, B.M., Lin, M.Y., Chou, S.L., Peng, Y.C.** Photoluminescence of Boron Nitride Nanosheets Exfoliated by Ball Milling *Applied Physics Letters* 100 (26) 2012: pp. 261108. https://doi.org/10.1063/1.4731203
24. **Zhang, F., Feng, Y., Feng, W.** Three-dimensional Interconnected Networks for Thermally Conductive Polymer Composites: Design, Preparation, Properties, and Mechanisms *Materials Science and Engineering: R: Reports* 142 2020: pp. 100580. https://doi.org/10.1016/j.mser.2020.100580

© Li et al. *2024* Open Access This article is distributed under the terms of the Creative Commons Attribution 4.0 International License (http://creativecommons.org/licenses/by/4.0/), which permits unrestricted use, distribution, and reproduction in any medium, provided you give appropriate credit to the original author(s) and the source, provide a link to the Creative Commons license, and indicate if changes were made.